Voltage-gated ion channels in the axon initial segment of human cortical pyramidal cells and their relationship with chandelier cells

Maria Carmen Inda*†, Javier DeFelipe†‡, and Alberto Muñoz*†

*Departamento de Biología Celular, Universidad Complutense de Madrid, Jose Antonio Novais 2, 28040 Madrid, Spain; and †Instituto Cajal, Consejo Superior de Investigaciones Cientificas, Avenida Doctor Arce 37, 28002 Madrid, Spain

Communicated by Edward G. Jones, University of California, Davis, CA, December 28, 2005 (received for review November 24, 2005)

The axon initial segment (AIS) of pyramidal cells is a critical region for the generation of action potentials and for the control of pyramidal cell activity. Here we show that Na^+ and K^+ voltage-gated channels, together with other molecules involved in the localization of ion channels, are distributed asymmetrically in the AIS of pyramidal cells situated in the human temporal neocortex. There is a high density of Na^+ channels distributed along the length of the AIS together with the associated proteins spectrin βIV and ankyrin G. In contrast, Kv1.2 channels are associated with the adhesion molecule Caspr2, and they are mostly localized to the distal region of the AIS. In general, the distal region of the AIS is targeted by the GABAergic axon terminals of chandelier cells, whereas the proximal region is innervated, mostly by other types of GABAergic interneurons. We suggest that this molecular segregation and the consequent regional specialization of the GABAergic input to the AIS of pyramidal cells may have important functional implications for the control of pyramidal cell activity.

inhibition | interneurons | neocortex

To understand how synaptic input is converted into neuronal output, it is first essential to fully comprehend the organization of the sites where the action potential is generated. Because of the high concentration of voltage-dependent Na^+ and K^+ channels in the axon initial segment (AIS), it has commonly been assumed that this region is the site with the lowest threshold, and, as such, it must be the first site at which the action potential is generated. However, some studies have suggested that action potentials initiate beyond the AIS (1, 2). Indeed, it has been shown recently that action potentials in cortical layer V pyramidal cells (3) and Purkinje cells of the cerebellum (4) are first generated at the first node of Ranvier. Under these circumstances, voltage-dependent Na^+ channels in the AIS would serve to back-propagate action potentials into the soma and dendrites. Differences in the action potential threshold between the AIS and the nodes of Ranvier might depend on axial resistivity, the diameter, length, and the density of voltage-dependent Na^+ channels (5). Furthermore, the different biophysical properties of ion channels in the AIS and nodes of Ranvier might reflect the differences in the distribution of voltage-dependent Na^+ and K^+ channels or in the molecular isoforms expressed in these structures. Such variations might determine the threshold for the initiation of the action potential at each site.

Chandelier cells are a particular type of GABAergic interneuron whose axon terminals [chandelier cell axon terminals (Ch-terminals)] specifically contact the AIS of cortical pyramidal cells. Alterations in the connectivity of chandelier cells have been associated with syndromes such as epilepsy (6) and schizophrenia (7), and it has traditionally been presumed that chandelier cells are key elements that control the output of pyramidal cells (1, 8–10). However, if action potentials are initiated in the first node of Ranvier, they would be propagated in a retrograde manner to the AIS, where they can be reproduced and back-propagated to the soma and dendrites. In this case, GABAergic synapses established by chandelier cells would not only control the output of pyramidal cells but also influence the back-propagation of action potentials, modulating the integration of information in the soma and dendrites. In fact, recent studies have shown that rather than simply shunting action potentials in pyramidal cells, chandelier cells participate in complex activities such as the synchronization of the firing patterns of large populations of hippocampal pyramidal cells in different states of consciousness (11, 12).

Voltage-dependent Na^+ and K^+ channels are spatially segregated and symmetrically distributed at the nodes of Ranvier. Both in the central and peripheral nervous system, they are restricted to specific isolated membrane domains, the nodal and juxtaparanodal regions, respectively, which are separated by the paranodal region (13, 14). Their restricted and defined distribution is maintained by the expression of key molecules involved in defining the localization of ion channels. These molecules include proteins that interact with the cytoskeleton, such as the spectrin βIV and ankyrin G, and adhesion molecules such as Neurofascin, NrCAM, Caspr, and Caspr2. The presence of some of these molecules has also been reported in the AIS of cerebellar Purkinje cells and of cortical cells in the rat, together with other molecules that regulate pyramidal cell excitability such as 5-HT_{1A} and $GABA_B$ receptors in humans and KCNQ2/3 channels in rats (15–20). However, the precise distribution of voltage-dependent Na^+ and K^+ channels and related molecules in the pyramidal cell AIS and their spatial relationship with the GABAergic Ch-terminals has not yet been explored.

In the present study, we have examined the relationship between Ch-terminals and the regional distribution of both voltage-dependent Na^+ and K^+ channels and associated proteins such as spectrin βIV, ankyrin G, and Caspr2 in the AIS of pyramidal cells in the human temporal neocortex. The results indicate that these molecules are distributed asymmetrically in the AIS, displaying a partial spatial segregation. Furthermore, we found that chandelier cells mostly innervated the distal region of the AIS, a domain that is characterized by a high density of K^+ channels.

Results

Voltage-Gated Na^+ Channels (VGSC). When we analyzed the distribution of VGSC in layers II–VI of the neocortex, numerous strongly labeled VGSC-immunoreactive (ir) AISs were observed (Figs. 1 and 2*A*), but no somata or dendrites were labeled. Indeed, they were so numerous that although we did not attempt

Conflict of interest statement: No conflicts declared.

Freely available online through the PNAS open access option.

Abbreviations: AIS, axon initial segment; Ch-terminals: chandelier cell axon terminals; ir, immunoreactive; VGSC, voltage-gated Na^+ channels.

‡To whom correspondence should be addressed. E-mail: defelipe@cajal.csic.es.

 www.pnas.org/cgi/doi/10.1073/pnas.0511197103

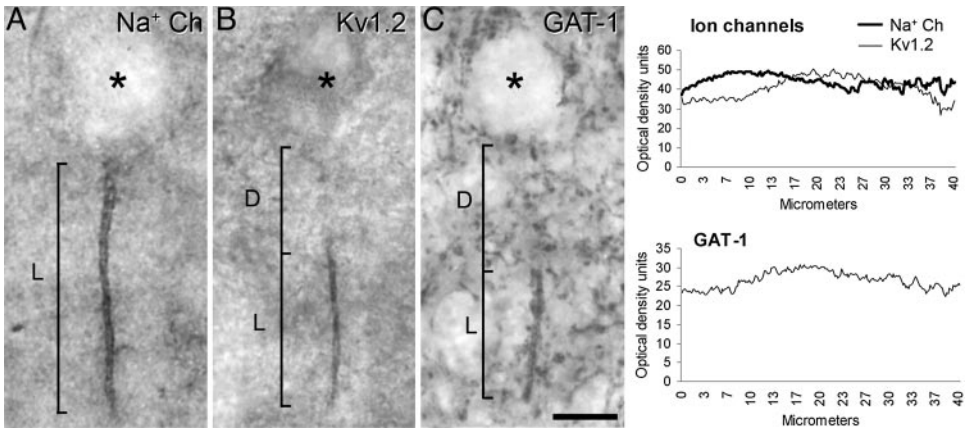

Fig. 1. Distribution of Na^+ and K^+ voltage channels in the AIS of pyromidal cells and their relationship with Ch-terminals. (*A* and *B*) Photomicrographs showing the AIS of pyramidal cells from the human temporal neocortex immunostained for VGSC (*A*) and Kv1.2 (*B*). (*C*) Photomicrograph showing a GAT-1-ir Ch-terminal. In *A* and *B*, L indicates how the length of the VGSC- and Kv1.2-ir AIS was measured, respectively. In *C*, L indicates the length of the GAT-1-ir Ch-terminal. D indicates the distance from the base of the pyramidal cell body to the beginning of the AIS labeled for Kv1.2 (*B*) or to the GAT-1-ir Ch-terminal (*C*). The asterisks indicate the location of pyramidal cell bodies. (Scale bar: 10 μm.) (*C Right*) The plots shown are presented as a function of the mean distance from the cell body based on optical density readings of the immunostaining for Na^+ and Kv1.2 channels along the AIS (*Upper*) or for GAT-1 Ch-terminals (*Lower*). Note that immunostaining for the VGSC is present along the whole length of the AIS, whereas for Kv1.2, the staining is restricted to the distal region of the AIS that is contacted by GAT-1-ir Ch-terminals (See Fig. 3 *D–F*).

to perform a quantitative study, it appeared that the AISs of all neurons were VGSC-positive. The labeled AISs extended distally for ≈11–40 μm (mean length ± SD: 23.12 ± 7.05 μm; n = 180 in layer III) from their somata of origin.

Spectrin βIV. Whereas spectrin βIV immunoreactivity was weak in the soma of pyramidal cells, the AISs of these cells were intensely labeled (Fig. 2 *B* and *E*). The spectrin βIV immunostaining in the AIS extended distally from the somata of origin for ≈11–47 μm (mean length ± SD: 25.6 ± 6.8; n = 212 in layer III). In double-labeling experiments, nearly all AISs in layer III that were labeled for VGSC (136 of 138; 98.5%) were also immunoreactive for spectrin βIV (Fig. 2 *A–C*).

Ankyrin G. Ankyrin G immunocytochemistry labeled the AIS of relatively few cells, although numerous dendritic processes were labeled, as were the somata of a sparse population of pyramidal neurons distributed through layers II–VI (Fig. 2*D*). Only the AISs in 23 of 163 spectrin βIV-ir cells (14%) were immunostained for ankyrin-G (Fig. 2 *D–F*). Thus, ankyrin G immunocytochemistry labels the AIS of a subpopulation of pyramidal cells that coexpress VGSC and spectrin βIV.

GAT-1 Labeling of Ch-Terminals. GAT-1-ir Ch-terminals (Figs. 1, 2*H*, and 3*E*) ranged in length from 10 to 39 μm in layer III (mean length ± SD: 22.2 ± 5.5 μm; n = 210), and they were usually located ≈8–19 μm (mean distance ± SD: 13.4 ± 2.8 μm; n = 22) below the unstained somata of the pyramidal cells from which the AIS innervated by the GAT-1-ir Ch-terminals originated. In sections double-labeled for GAT-1 and VGSC, the GAT-1-ir Ch-terminals surrounded most VGSC-ir pyramidal cell axons (Fig. 2 *G–I*). Moreover, it was clear that there was a regional specialization of the AIS because VGSC immunoreactivity was distributed along the length of the AIS from the somata, whereas the majority of GAT-1-ir Ch-terminals only innervated the distal region of the VGSC-ir AIS (Fig. 2 *G–I*).

Kv1.2. Kv1.2 immunocytochemistry revealed the presence of numerous labeled AISs in all cortical layers (Figs. 1 and 3 *A* and *D*). In layer III, these Kv1.2-ir AISs ranged in length from 7 to 27 μm (mean length ± SD: 14.82 ± 4.54 μm; n = 116). However, Kv1.2 immunostaining did not extend along the whole length of the AIS; rather it was confined to the more distal region (Fig. 3 *A–D*).

Caspr2. Caspr2 immunocytochemistry also labeled numerous AISs ranging in length from 11 to 26 μm (mean length ± SD: 15.85 ± 3.12 μm; n = 79 in layer III) with a similar pattern to that observed for Kv1.2. Indeed, in sections labeled for both Kv1.2 and Caspr2, the immunostaining for Caspr2 was specific to the distal AIS in perfect register with the distribution of Kv1.2 (Fig. 3 *A–C*). Of the AISs that were labeled by antibodies against Kv1.2, 92% were also labeled for Caspr2. Indeed, labeling for Caspr2 failed to coincide with that for Kv1.2 in only 8 of 99 AISs labeled for Kv1.2. Furthermore, in sections double-labeled for Kv1.2 and GAT-1, Kv1.2 channels were restricted to the distal region of the AIS in register with the region that is innervated by GAT-1-ir Ch-terminals (Fig. 3 *D–F*). It should be noted that VGSC and Caspr2 also colocalized in the AIS of the majority of pyramidal cells in double-labeled sections. Only 3 of 102 VGSC-ir AISs were not labeled by antibodies against Caspr2. Therefore, both VGSC and Kv1.2 overlapped in the distal AIS, whereas the proximal AISs were characterized by the presence of VGSC and the absence of Kv1.2 (Figs. 2 and 3) and Ch-terminals.

Discussion

The basis for the generation and saltatory propagation of action potentials is the exquisite molecular architecture of nerve fibers, notably in the segregation of voltage-gated ion channels into distinct membrane domains (13, 21–24). This segregation is achieved through specific sorting mechanisms coupled to the anchoring and clustering of these proteins in the plasma membrane. The ion channels that underlie excitability are compartmentalized into sharply defined subcellular regions and form heteromultimeric complexes that also contain intracellular scaffolding, adapter, and cytoskeleton proteins, transmembrane proteins, and extracellular matrix elements (see below). The similarities in the membranes of the AIS and the nodes of Ranvier (25, 26) extend to the presence of an electron-dense membrane undercoat that is necessary to cluster the voltage-gated ion channels (27). However, whereas the molecular architecture of the nodes of Ranvier has been extensively studied in the rat CNS and peripheral nervous system, much less is known

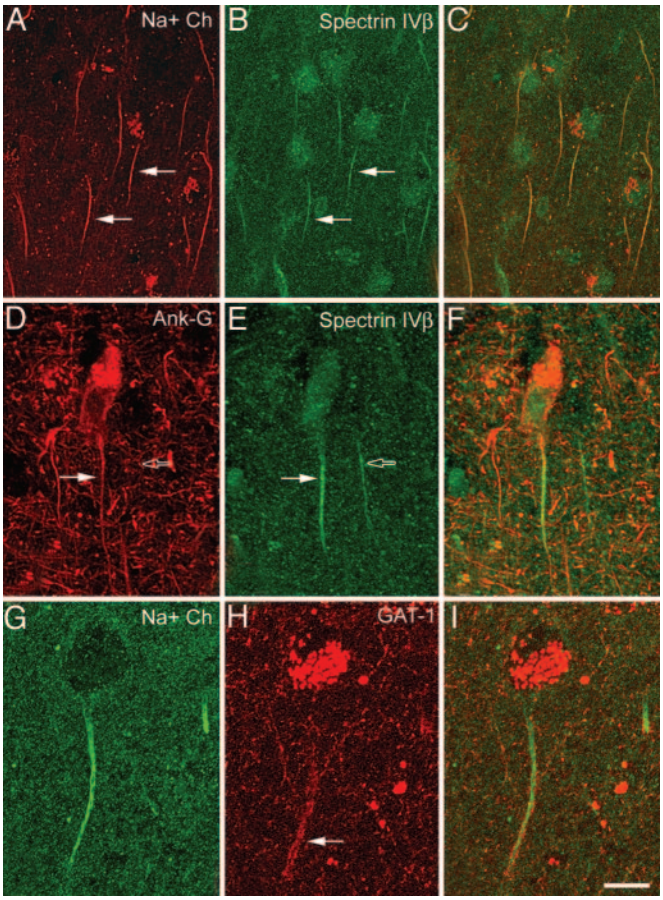

Fig. 2. Confocal images from the same section and microscopic field illustrating double labeling for VGSC (Na^+ Ch) and spectrin βIV (*A–C*), ankyrin G and spectrin βIV (*D–F*), and VGSC and GAT-1 (*G–I*) in the AIS of pyramidal cells from the human temporal neocortex. *C*, *F*, and *I* were obtained after combining images *A* and *B*, *D* and *E*, and *G* and *H*, respectively. Note the colocalization of VGSC and spectrin βIV (filled arrows in *A* and *B*) and of ankyrin G and spectrin βIV (filled arrows in *D* and *E*) in the AIS of pyramidal cells. Open arrows in *D* and *E* point to the AIS of a pyramidal cell immunoreactive for spectrin βIV, which does not colocalize ankyrin G. Note in *G–I* that the VGSC are distributed along the length of the AIS from the somata, whereas the GAT-1-ir Ch-terminals (filled arrow in *H*) innervate only the distal region of the AIS. Images *A–C* represent stacks of 15 optical sections obtained at a distance of 1.5 μm in the *z* axis (total: 22 μm). Images *D–F* represent stacks of seven optical sections obtained at a distance of 1.4 μm in the *z* axis (total: 9 μm). Images *G–I* represent stacks of six optical sections obtained at a distance of 1.3 μm in the *z* axis (total: 7 μm). (Scale bar: *A–C*, 25 μm; *D–I*, 15 μm.)

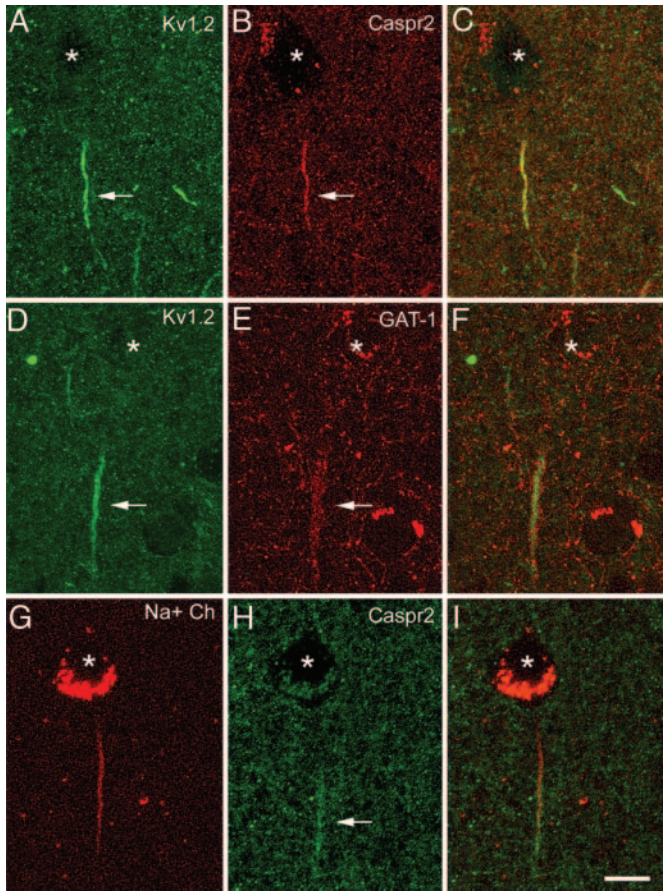

Fig. 3. Confocal images from the same section and microscopic field illustrating double labeling for Kv1.2 and Caspr2 (*A–C*), Kv1.2 and GAT-1 (*D–F*), and VGSC and Caspr2 (*G–I*) in the human temporal neocortex. The asterisks indicate the location of the pyramidal cell bodies. *C*, *F*, and *I* were obtained after combining the images *A* and *B*, *D* and *E*, and *G* and *H*, respectively. Note that Kv1.2 immunostaining is confined to the distal region of the AIS where Caspr2 is also expressed (filled arrows in *A* and *B*). This distal AIS specifically receives GABAergic innervation from the GAT-1-ir Ch-terminals (filled arrows in *D* and *E*). VGSC and Kv1.2 partially overlap at the distal AIS (filled arrow in *F*), whereas the proximal AIS is characterized by the presence of VGSC and the absence of Kv1.2 (*D–I*). Images *A–C* represent stacks of nine optical sections obtained at a distance of 1.1 μm in the *z* axis (total: 9 μm). Images *D–F* and *G–I* represent stacks of four optical sections obtained at a distance of 1.1 μm in the *z* axis (total: 3 μm). (Scale bar: 11 μm.)

about the AIS. We present a morphological description of the distribution of voltage-dependent Na^+ and K^+ channels in the AIS of human pyramidal cells. The results indicate that some features observed in the AIS are common to the nodes of Ranvier, particularly regarding the molecules with which ion channels may associate. However, the results also indicate fundamental differences in ion channel distribution between the AIS and the nodes of Ranvier.

VGSC. VGSC are responsible for the rapid inward sodium currents and the consequent depolarization required for the induction of the action potential and saltatory conduction (28, 29). The anti-pan-sodium channel antibody used in the present study recognizes all of the known vertebrate Na^+ channel isoforms (30), and, therefore, it is thought to reflect the complete repertoire of VGSC in the AIS, where they are distributed along its whole length. At the nodal region of the nodes of Ranvier, VGSC are clustered at a high density. In these structures, they are associated with the underlying actin-spectrin cytoskeleton through the adaptor protein ankyrin G and to NrCAM and neurofascin 186, nodal cell adhesion molecules of the Ig superfamily (13, 14). The same molecular interactions seem to occur in the AIS in different neuronal populations of the rat CNS, where NrCAM and neurofascin 186 have been shown to be concentrated (18, 31–35). In addition, spectrin βIV has been seen to concentrate at the AISs of both neocortical and hippocampal cells, where it might be involved in the localization of VGSC and ankyrin G (19, 36, 37). In keeping with these studies, the AISs of human neocortical pyramidal cells express VGSC and spectrin βIV, which colocalize along the length of the AIS in virtually all pyramidal cells. However, we observed little colocalization with ankyrin G. The antibody used in the present study to recognize ankyrin G identifies a single protein of between 200 and 300 kDa that might correspond to only one of the established nodal isoforms (270 kDa). Hence, it may not recognize the 480-kDa (33, 34, 38) or the 97-kDa (39, 40)

isoforms previously identified as nodal components in the CNS. Therefore, because the 270-kDa isoform of ankyrin G seems to be present in only ≈15% of the human neocortical pyramidal cells (this study), different ankyrin G polypeptides or other anchoring proteins might participate in the clustering of VGSC in the AIS of specific pyramidal cell populations.

Voltage-Dependent K^+ Channels. Voltage-dependent K^+ channels of the Kv1 subfamily of *Shaker*-type delayed-rectifying K^+ channels are present at the nodes of Ranvier where they are found in the juxtaparanodal axonal membrane beneath the overlying compact myelin (41–44). Kv1 channels generate low-threshold voltage-dependent outward currents that seem to regulate the action potential threshold. They contribute to the repolarization of single-action potentials, they modulate action potential duration and frequency, and they maintain the internodal resting potential (29, 34, 45, 46). Juxtaparanodal Kv channels are composed of various heteromultimeric combinations of pore-forming Kv1 α (Kv 1.1, 1.2, 1.4, and 1.6) and the associated cytoplasmic Kvβ2 subunits (42, 44, 47, 48). In the juxtaparanodal region, Kv1.1 and Kv1.2 have been shown to colocalize with, and to interact and/or cluster with, Caspr2, a member of the neurexin superfamily (49, 50). Indeed Caspr2 also interacts with other proteins necessary for the accumulation of Kv channels at the juxtaparanodal region and for their interaction with the actin–spectrin cytoskeleton (14, 51–56). The present results show that in human neocortical pyramidal cells, Kv1.2 channels are clustered at and colocalize with the adhesion molecule Caspr2 exclusively in the distal domain of the AIS. This region of the AIS is innervated by Ch-terminals, and it is therefore devoid of myelin. In contrast, Kv1.2 is located beneath the compact myelin sheath at the juxtaparanodes. Whether Caspr2 or other adhesion molecules that might be present at the distal region of the AIS specifically interact with the adhesion molecules of Ch-terminals is a possibility that should be further evaluated.

Differential Distribution of Voltage-Dependent Na^+ and K^+ Channels at the AIS and the Node of Ranvier. At the nodes of Ranvier, VGSC and Kv1.2 are symmetrically distributed and spatially segregated. Indeed, VGSC and Kv1.2 are confined to the nodal and juxtaparanodal regions, respectively, separated by the paranodal region (14, 24). The present results show that in contrast to the nodes of Ranvier, voltage-dependent Na^+ and K^+ channels are only partially segregated in the AIS and that there is a certain degree of overlap in the distal portion of the AIS. Whether this difference might be relevant to define the physiological attributes of action potentials generated in the AIS when compared to those in the nodes of Ranvier should be further studied.

The spatial distribution of ion channels is another relevant molecular difference between the nodes of Ranvier and the AIS. At the nodes of Ranvier, ion channels are symetrically distributed, and VGSC in the nodal region are flanked by K^+ channels expressed in the juxtaparanodal regions. In contrast, in the AIS, the Kv1.2 channels are exclusively found in the distal domain where VGSC are expressed. It is important to note that over the first 3 weeks of postnatal development in the rat peripheral nervous system, Kv1 channel clustering is often asymmetrical (50%), and channels may be found exclusively in the distal juxtaparanode (46). However, this asymmetrical distribution is transient, lasting only until the end of the third postnatal week, and it may lead to instabilities in the propagation of the action potential (46). Thus, it is of interest to determine what the functional consequences of the asymmetrical distribution of voltage-gated Na^+ and K^+ channels are in the AIS of human neocortical cells. This distribution may be particularly relevant to the generation of the action potential and for the directionality of action potential transmission.

Modulation of Action Potential Firing at the AIS by Chandelier Cells. In different neuronal types, including Purkinje cells of the cerebellum (4) and pyramidal cells of the subiculum (1) and neocortex (3), it has been shown that action potentials are first generated beyond the AIS. Indeed, this event occurs at the first node of Ranvier, which shows a lower threshold for the initiation of the action potential. Action potentials generated at distal axonal locations then invade the soma and dendrites, a process that depends on the presence of VGSC at the AIS that serve to back-propagate action potentials into the soma and dendrites (1–5). Inhibition of the AIS by GABAergic inputs from chandelier cells or through other neurotransmitters would dissociate the soma from the site of action potential initiation. As a result, it would not only be suited for orthodromic inhibition that would simply suppress the initiation of the action potential but also for antidromic inhibition. This latter type of inhibition might have important consequences in controlling the back-propagation of action potentials, influencing the level of neuronal output to the soma and the dendritic tree that is necessary for the integration of information (57). In fact, recent studies indicate that chandelier cells, together with other interneurons, are involved in complex activities. These actions contribute to ensuring well timed hyperpolarization that regulates the firing of pyramidal cells and shapes the network output and the rhythms generated in different states of consciousness (11, 12, 58–61).

The present study shows that Ch-terminals innervate the distal region of the AIS where voltage-gated K^+ channels are located. On the other hand, the proximal region of the AIS shows a high density of VGSC, which seem to be less accessible to the inhibitory influence of Ch-terminals. This proximal region is likely to be innervated by other types of interneurons that occasionally form synapses with the AIS (62, 63). The precise point at which the action potential is initiated in human cortical cells is not yet known. Nevertheless, it seems that inhibition by the selective innervation of the distal AIS by Ch-terminals in human pyramidal cells might be directionally selective (60), being more effective from either the soma to the axon or vice versa. This directional selectivity, and the consequent pattern of action potential firing and back-propagation in pyramidal cells, might vary depending on the regulation of K^+ conductances at the AIS by different neurotransmitter systems such as the serotonergic and cholinergic ascending systems (17, 39, 40, 64). These regulatory systems, together with chandelier cells and other types of GABAergic interneurons, might modify the physiological requirements for the generation of action potentials and, possibly, the location at which the action potential is initiated in human pyramidal cells. This regulation may occur through their direct action on the AIS, an intriguing possibility that has to be evaluated in further studies.

Materials and Methods

Human neocortical tissue from the anterolateral temporal cortex was obtained by surgical resection from one male and four female patients diagnosed with intractable temporal lobe epilepsy with a mesial origin (age range = 21–54 years). All patients were evaluated presurgically by scalp electroencephalography (EEG), interictal single-photon emission computer tomography, magnetic resonance imaging (MRI) 1.5 T, and videoelectroencephalography that included the use of 19 scalp electrodes placed according to the international 10–20 system and foramen-ovale electrodes. Informed consent was obtained individually for all patients, having been previously approved by ethical committee of the "Hospital de la Princesa" (Madrid). During surgery, electrocorticography was performed with a grid of 4 × 5 electrodes embedded in Sylastic. The electrodes were placed directly over the exposed lateral temporal cortex, and they were of 1.2 mm in diameter with a 1 cm center-to-center interelectrode distance (Add-Tech, Racine, WI). Recordings were sam-

pled at 400 Hz with a bandwidth of 1–70 Hz and over a minimum period of 20 min, by using a 32-channel Easy EEG II system (Cadwell, Kennewick, WA). Spiking areas were identified as electrodes showing spikes (<80 ms) or sharp waves (80–200 ms) with a mean frequency >1 spike/min. Nonspiking areas were defined as electrodes where no spikes, sharp waves, or slow activity was observed. Photographs of the placement of the electrodes were taken before grid removal, and the anatomical location of the spiking and nonspiking areas was defined before tissue excision.

In all cases, tailored temporal lobectomy and amygdalohippocampectomy was performed under electrocorticography guidance. After surgery, the lateral neocortex and mesial structures were subjected to standard neuropathological assessment. All of the lateral neocortical biopsies were histologically normal, whereas the hippocampal formation displayed neuronal loss and gliosis (hippocampal sclerosis). In the present study, only normal nonspiking areas of the lateral neocortex were used. Biopsy samples were fixed in cold 4% paraformaldehyde in 0.1 M phosphate buffer at pH 7.4 (PB) for 4–5 h at 4°C. Vibratome sections (100 μm thick) were immunolabeled by using the following antibodies: mouse anti-Na^+ channels (1:100; Sigma), mouse anti-K^+ channel Kv1.2 (1:50; Upstate Biotechnology, Lake Placid, NY), mouse anti-ankyrin G (1:150; Zymed), chicken anti-spectrin βIV (1:100, gift from M. Komada, Tokyo Institute of Technology, Yokohama, Japan; see ref. 19), rabbit anti-GAT-1 (1:500; Chemicon), and rabbit anti-Caspr2 (1:250; United States Biological).

The mouse anti-Na^+ channel antibody used was raised against a synthetic peptide derived from the intracellular III-IV loop of Na^+ channel, which is identical in all known vertebrate Na^+ channels. Mouse Kv1.2 antibodies were generated against a fusion protein corresponding to amino acids 428–499 of rat heart Kv1.2, and they recognize the Shaker-related α-subunit Kv1.2 in different species, including humans. Chicken anti-βIV spectrin antibodies were raised against the variable region (amino acids 2,171–2,345 of βIV e1-spectrin) expressed in *Escherichia coli* as a glutathione *S*-transferase fusion protein (19). Mouse anti-ankyrin G antibodies were raised against a synthetic peptide derived from the spectrin-binding domain of the human ankyrin G protein. These antibodies identify a single protein of between 200 and 300 kDa on Western blots, react with all splice forms of ankyrin G containing a spectrin-binding domain, and do not cross-react with related ankyrin isoforms. Rabbit anti-Caspr2 was raised against a C-terminus peptide corresponding to intracellular amino acid residues 1,315–1,331 of human Caspr2. Rabbit anti-GAT-1 was generated against a C-terminus peptide (amino acids 588–599) of the rat GAT-1.

Sections were single-labeled or double-labeled by using the following combinations of primary antibodies: Na^+ channels with spectrin βIV, ankyrin G, Caspr2, and GAT-1 or Kv1.2 with Caspr2 and GAT-1. The sections were then rinsed and incubated for 2 h at room temperature in biotinylated secondary antibodies directed against one of the primary antibodies used in each combination (rabbit anti-chicken, goat anti-rabbit, horse anti-mouse, or rabbit anti-goat as appropriate). After rinsing in PB, the sections were incubated for 2 h at room temperature in streptavidin coupled to Alexa Fluor 488 (1:1,000; Molecular Probes) and goat anti-mouse or goat anti-rabbit coupled to Alexa 594 (1:1,000, Molecular Probes) directed against the other primary antibody used. The sections were then washed, mounted in 50% glycerol in PB, and examined with a Leica (Cambridge, U.K.) TCS 4D confocal laser scanning microscope. Z sections were recorded at 1–2 μm intervals through separate channels (Scanware; Leica). Subsequently, Micrografx PICTURE PUBLISHER (Dallas) and PHOTOSHOP (Adobe Systems, San Jose, CA) software were used to construct composite images from each series by combining the images recorded through both channels and to generate the figures.

Identification and Quantitative Analysis of the AIS and Ch-Terminals. The AIS was readily identified as a short, thin, and smooth process with a characteristic "eyelash-like" appearance (Fig. 1 *A* and *B*). In contrast, GAT-1-ir Ch-terminals were identified as short, vertical rows of buttons (65) that could be clearly distinguished from other labeled elements (Fig. 1*C*). The length of the labeled AIS and the Ch-terminals was measured on microphotographs at a final magnification of ×1,000 (Fig. 1). The somata from which the Na^+ channel-ir AIS originated were identified because the labeled AIS arose directly from the base of the unlabeled somata (Fig. 1*A*). The cells that gave origin to a Kv1.2-ir AIS were considered to be those unlabeled somata located just above the labeled AIS and in the same plane (Fig. 1*B*). Similarly, the somata of pyramidal cells whose AISs were innervated by GAT-1-ir Ch-terminals were considered to be those located immediately above the labeled Ch-terminal (Fig. 1*C*).

Fluorescence microscopy was used to measure the intensity of staining for the different markers along the AIS. The intensity of immunostaining for Na^+ and Kv1.2 channels along the AIS ($n = 26$ and 15, respectively) and for GAT-1-ir Ch-terminals ($n = 18$) was quantified by densitometry by using a 3- to 4-μm-width rectangular sampling tool (IMAGEJ software; Sun Microsystems, Santa Clara, CA), extending from the base of soma to the distal portion of the labeled AIS or Ch-terminal. The means were plotted as a function of the distance from the cell body (Fig. 1).

We thank Dr. Komada for providing the spectrin βIV antibody. This work was supported by "Ministerio de Educación y Ciencia" Grants BFI 2003-01018 (to A.M.) and BFI 2003-02745 (to J.D.).

1. Colbert, C. M. & Johnston, D. (1996) *J. Neurosci.* **16,** 6676–6686.
2. Stuart, G., Schiller, J. & Sakmann, B. (1997) *J. Physiol. (London)* **505,** 617–632.
3. Colbert, C. M. & Pan, E. (2002) *Nat. Neurosci.* **5,** 533–538.
4. Clark, B. A., Monsivais, P., Branco, T., London, M. & Hausser, M. (2005) *Nat. Neurosci.* **8,** 137–139.
5. Mainen, Z. F., Joerges, J., Huguenard, J. R. & Sejnowski, T. J. (1995) *Neuron* **15,** 1427–1439.
6. DeFelipe, J. (1999) *Brain* **122,** 1807–1822.
7. Lewis, D. A., Hashimoto, T. & Volk, D. W. (2005) *Nat. Rev. Neurosci.* **6,** 312–324.
8. Stuart, G. J. & Sakmann, B. (1994) *Nature* **367,** 69–72.
9. Buhl, E. H., Han, Z. S., Lorinczi, Z., Stezhka, V. V., Karnup, S. V. & Somogyi, P. (1994) *J. Neurophysiol.* **71,** 1289–1307.
10. Miles, R., Toth, K., Gulyas, A. I., Hajos, N. & Freund, T. F. (1996) *Neuron* **16,** 815–823.
11. Cobb, S. R., Buhl, E. H., Halasy, K., Paulsen, O. & Somogyi, P. (1995) *Nature* **378,** 75–78.
12. Klausberger, T., Marton, L. F., Baude, A., Roberts, J. D., Magill, P. J. & Somogyi, P. (2004) *Nat. Neurosci.* **7,** 41–47.
13. Arroyo, E. J. & Scherer, S. S. (2000) *Histochem. Cell Biol.* **113,** 1–18.
14. Poliak, S. & Peles, E. (2003) *Nat. Rev. Neurosci.* **4,** 968–980.
15. Winckler, B. & Mellman, I. (1999) *Neuron* **23,** 637–640.
16. Winckler, B., Forscher, P. & Mellman, I. (1999) *Nature* **397,** 698–701.
17. DeFelipe, J., Arellano, J. I., Gomez, A., Azmitia, E. C. & Munoz, A. (2001) *J. Comp. Neurol.* **433,** 148–155.
18. Jenkins, S. M. & Bennett, V. (2001) *J. Cell Biol.* **155,** 739–746.
19. Komada, M. & Soriano, P. (2002) *J. Cell Biol.* **156,** 337–348.
20. Ango, F., di Cristo, G., Higashiyama, H., Bennett, V., Wu, P. & Huang, Z. J. (2004) *Cell* **119,** 257–272.
21. Scherer, S. S. (1999) *Ann. N.Y. Acad. Sci.* **883,** 131–142.
22. Peles, E. & Salzer, J. L. (2000) *Curr. Opin. Neurobiol.* **10,** 558–565.
23. Scherer, S. S. & Arroyo, E. J. (2002) *J. Peripher. Nerv. Syst.* **7,** 1–12.
24. Salzer, J. L. (2003) *Neuron* **40,** 297–318.
25. Palay, S. L., Sotelo, C., Peters, A. & Orkand, P. M. (1968) *J. Cell Biol.* **38,** 193–201.
26. Peters, A., Proskauer, C. C. & Kaiserman-Abramof, I. R. (1968) *J. Cell Biol.* **39,** 604–619.
27. Matsumoto, E. & Rosenbluth, J. (1985) *J. Neurocytol.* **14,** 731–747.

28. Catterall, W. A. (2000) *Neuron* **26,** 13–25.
29. Hille, B. (2001) *Ion Channels of Excitable Membranes* (Sinauer Associates, Sunderland, MA).
30. Rasband, M. N., Peles, E., Trimmer, J. S., Levinson, S. R., Lux, S. E. & Shrager, P. (1999) *J. Neurosci.* **19,** 7516–7528.
31. Davis, J. Q., McLaughlin, T. & Bennett, V. (1993) *J. Cell Biol.* **121,** 121–133.
32. Davis, J. Q., Lambert, S. & Bennett, V. (1996) *J. Cell Biol.* **135,** 1355–1367.
33. Lambert, S., Davis, J. Q. & Bennett, V. (1997) *J. Neurosci.* **17,** 7025–7036.
34. Zhou, D., Lambert, S., Malen, P. L., Carpenter, S., Boland, L. M. & Bennett, V. (1998) *J. Cell Biol.* **143,** 1295–1304.
35. Tait, S., Gunn-Moore, F., Collinson, J. M., Huang, J., Lubetzki, C., Pedraza, L., Sherman, D. L., Colman, D. R. & Brophy, P. J. (2000) *J. Cell Biol.* **150,** 657–666.
36. Berghs, S., Aggujaro, D., Dirkx, R., Jr., Maksimova, E., Stabach, P., Hermel, J. M., Zhang, J. P., Philbrick, W., Slepnev, V., Ort, T., *et al.* (2000) *J. Cell Biol.* **151,** 985–1002.
37. Lacas-Gervais, S., Guo, J., Strenzke, N., Scarfone, E., Kolpe, M., Jahkel, M., De Camilli, P., Moser, T., Rasband, M. N. & Solimena, M. (2004) *J. Cell Biol.* **166,** 983–990.
38. Zhang, X. & Bennett, V. (1996) *J. Biol. Chem.* **271,** 31391–31398.
39. Devaux, J., Alcaraz, G., Grinspan, J., Bennett, V., Joho, R., Crest, M. & Scherer, S. S. (2003) *J. Neurosci.* **23,** 4509–4518.
40. Devaux, J. J., Kleopa, K. A., Cooper, E. C. & Scherer, S. S. (2004) *J. Neurosci.* **24,** 1236–1244.
41. Chiu, S. Y. & Ritchie, J. M. (1980) *Nature* **284,** 170–171.
42. Wang, H., Kunkel, D. D., Martin, T. M., Schwartzkroin, P. A. & Tempel, B. L. (1993) *Nature* **365,** 75–79.
43. Wang, H., Kunkel, D. D., Schwartzkroin, P. A. & Tempel, B. L. (1994) *J. Neurosci.* **14,** 4588–4599.
44. Mi, H., Deerinck, T. J., Ellisman, M. H. & Schwarz, T. L. (1995) *J. Neurosci.* **15,** 3761–3774.
45. Smart, S. L., Lopantsev, V., Zhang, C. L., Robbins, C. A., Wang, H., Chiu, S. Y., Schwartzkroin, P. A., Messing, A. & Tempel, B. L. (1998) *Neuron* **20,** 809–819.
46. Vabnick, I., Trimmer, J. S., Schwarz, T. L., Levinson, S. R., Risal, D. & Shrager, P. (1999) *J. Neurosci.* **19,** 747–758.
47. Hopkins, W. F., Demas, V. & Tempel, B. L. (1994) *J. Neurosci.* **14,** 1385–1393.
48. Rhodes, K. J., Strassle, B. W., Monaghan, M. M., Bekele-Arcuri, Z., Matos, M. F. & Trimmer, J. S. (1997) *J. Neurosci.* **17,** 8246–8258.
49. Poliak, S., Gollan, L., Martinez, R., Custer, A., Einheber, S., Salzer, J. L., Trimmer, J. S., Shrager, P. & Peles, E. (1999) *Neuron* **24,** 1037–1047.
50. Poliak, S., Gollan, L., Salomon, D., Berglund, E. O., Ohara, R., Ranscht, B. & Peles, E. (2001) *J. Neurosci.* **21,** 7568–7575.
51. Rasband, M. N., Park, E. W., Zhen, D., Arbuckle, M. I., Poliak, S., Peles, E., Grant, S. G. & Trimmer, J. S. (2002) *J. Cell Biol.* **159,** 663–672.
52. Traka, M., Dupree, J. L., Popko, B. & Karagogeos, D. (2002) *J. Neurosci.* **22,** 3016–3024.
53. Traka, M., Goutebroze, L., Denisenko, N., Bessa, M., Nifli, A., Havaki, S., Iwakura, Y., Fukamauchi, F., Watanabe, K., Soliven, B., *et al.* (2003) *J. Cell Biol.* **162,** 1161–1172.
54. Poliak, S., Salomon, D., Elhanany, H., Sabanay, H., Kiernan, B., Pevny, L., Stewart, C. L., Xu, X., Chiu, S. Y., Shrager, P., *et al.* (2003) *J. Cell Biol.* **162,** 1149–1160.
55. Girault, J. A., Oguievetskaia, K., Carnaud, M., Denisenko-Nehrbass, N. & Goutebroze, L. (2003) *Biol. Cell* **95,** 447–452.
56. Denisenko-Nehrbass, N., Oguievetskaia, K., Goutebroze, L., Galvez, T., Yamakawa, H., Ohara, O., Carnaud, M. & Girault, J. A. (2003) *Eur. J. Neurosci.* **17,** 411–416.
57. Stuart, G., Spruston, N., Sakmann, B. & Hausser, M. (1997) *Trends Neurosci.* **20,** 125–131.
58. Whittington, M. A. & Traub, R. D. (2003) *Trends Neurosci.* **26,** 676–682.
59. Klausberger, T., Magill, P. J., Marton, L. F., Roberts, J. D., Cobden, P. M., Buzsaki, G. & Somogyi, P. (2003) *Nature* **421,** 844–848.
60. Howard, A., Tamas, G. & Soltesz, I. (2005) *Trends Neurosci.* **28,** 310–316.
61. Somogyi, P. & Klausberger, T. (2005) *J. Physiol.* **562,** 9–26.
62. Farinas, I. & DeFelipe, J. (1991) *J. Comp. Neurol.* **304,** 70–77.
63. Gonchar, Y., Turney, S., Price, J. L. & Burkhalter, A. (2002) *J. Comp. Neurol.* **443,** 1–14.
64. Cooper, E. C., Harrington, E., Jan, Y. N. & Jan, L. Y. (2001) *J. Neurosci.* **21,** 9529–9540.
65. DeFelipe, J. & Gonzalez-Albo, M. C. (1998) *NeuroReport* **9,** 467–470.